Articles

Electronic Interactions in Iron- and Ruthenium-Containing Heterobimetallic Complexes: Structural and Spectroscopic Investigations

Daniel Serra, Khalil A. Abboud, Casie R. Hilliard, and Lisa McElwee-White*

Department of Chemistry and Center for Catalysis, University of Florida, Gainesville, Florida 32611-7200

Received November 24, 2006

The heterobimetallic Ru complexes Cp(CO)Ru(μ-I)(μ-dppm)PtI_2 (**8**), Cp(CO)Ru(μ-I)(μ-dppm)PdI_2 (**10**), and Cp(CO)RuI(μ-dppm)AuI (**12**) and their isoelectronic Fe analogues Cp(CO)Fe(μ-I)(μ-dppm)PtI_2 (**9**), Cp(CO)Fe(μ-I)(μ-dppm)PdI_2 (**11**), and Cp(CO)FeI(μ-dppm)AuI (**13**) were prepared by the reactions of Cp(CO)M(κ^1-dppm)I (**6**, M = Ru; **7**, M = Fe) with Pt(COD)I_2, Pd(COD)I_2, and AuI, respectively. All six complexes were characterized by cyclic voltammetry, IR, UV, and NMR (^{1}H and ^{31}P) spectroscopy, and elemental analysis. The structures of the I-bridged compounds **8**−**11** were determined by X-ray crystallography. Electronic interaction between the two metals is significant for the iodide-bridged compounds **8**−**11**, as evidenced by the variation in their carbonyl stretching frequencies and UV−vis spectra, as well as in the shifts of their redox potentials in comparison to the shifts for mononuclear model compounds. In contrast, compounds **12** and **13**, which have only dppm bridges, exhibit limited interactions between the two metals.

Introduction

The chemistry of heterobimetallic complexes has attracted attention, due to the possibility of combining the different reactivities of the two metals in chemical transformations.[1−7] It has been long recognized that interesting characteristics such as cooperative behavior and/or different mechanistic roles of the metal centers can be observed when two metals are in close proximity.[2,8−14] It has also been shown that the cooperative effect in heterobimetallic complexes can enhance catalytic activities or can result in unique properties not observed in monomeric models.[12,15−19]

A similar effect has been noted for the electrooxidation of methanol upon comparison of various electrode materials:[20−22] initially Pt anodes[23−25] and then more complex alloys.[25−32]

(1) Braunstein, P.; Rose, J. In *Comprehensive Organometallic Chemistry II*; Abel, E. W., Stone, F. G. A., Wilkinson, G., Eds.; Pergamon: Oxford, U.K., 1995; Vol. 10, p 351.
(2) *Catalysis by Di- and Polynuclear Metal Cluster Complexes*; Adams, R. D., Cotton, F. A., Eds.; Wiley-VCH: New York, 1998.
(3) Suss-Fink, G.; Meister, G. In *Advances in Organometallic Chemistry*; Stone, F. G. A., West, R., Eds.; Academic Press: New York, 1993; Vol. 35, pp 41−134.
(4) Van Den Beuken, E. K.; Feringa, B. L. *Tetrahedron* **1998**, *54*, 12985−13011.
(5) Wheatley, N.; Kalck, P. *Chem. Rev.* **1999**, *99*, 3379−3419.
(6) Xia, B. H.; Zhang, H. X.; Che, C. M.; Leung, K. H.; Phillips, D. L.; Zhu, N. Y.; Zhou, Z. Y. *J. Am. Chem. Soc.* **2003**, *125*, 10362−10374.
(7) Jones, N. D.; James, B. R. *Adv. Synth. Catal.* **2002**, *344*, 1126−1134.
(8) McCollum, D. G.; Bosnich, B. *Inorg. Chim. Acta* **1998**, *270*, 13−19.
(9) Bosnich, B. *Inorg. Chem.* **1999**, *38*, 2554−2562.
(10) Stephan, D. W. *Coord. Chem. Rev.* **1989**, *95*, 41−107.
(11) Adams, R. D.; Barnard, T. S. *Organometallics* **1998**, *17*, 2885−2890.
(12) Quebatte, L.; Scopelliti, R.; Severin, K. *Eur. J. Inorg. Chem.* **2006**, 231−236.
(13) Cornelissen, C.; Erker, G.; Kehr, G.; Fröhlich, R. *Organometallics* **2005**, *24*, 214−225.
(14) McCleverty, J. A.; Ward, M. D. *Acc. Chem. Res.* **1998**, *31*, 842−851.
(15) Sinfelt, J. H. In *Bimetallic Catalysts: Discovery, Concepts, and Applications*; Wiley: New York 1983.
(16) Halpern, J. *Inorg. Chim. Acta* **1982**, *62*, 31−37.
(17) Gauthier, S.; Scopelliti, R.; Severin, K. *Organometallics* **2004**, *23*, 3769−3771.
(18) Ng, S. Y.; Goh, L. Y.; Koh, L. L.; Leong, W. K.; Tan, G. K.; Ye, S.; Zhu, Y. *Eur. J. Inorg. Chem.* **2006**, *2006*, 663−670.
(19) *Multimetallic Catalysts in Organic Synthesis*; Shibasaki, M., Yamamoto, Y., Eds.; Wiley-VCH: Weinheim, Germany, 2004.
(20) Iwasita, T. In *Advances in Electrochemical Science and Engineering*; Gerischer, H., Tobias, C., Eds.; Verlag Chemie: Weinheim, Germany, 1990; Vol. 1, pp 127−170.
(21) Hamnett, A. In *Interfacial Electrochemistry: Theory, Experimental and Applications*; Wieckowski, A., Ed.; Marcel Dekker: New York, 1999.
(22) Iwasita, T. *Electrochim. Acta* **2002**, *47*, 3663−3674.
(23) Enyo, M.; Machida, K.; Fukuaka, A.; Ichikawa, M. In *Electrochemistry in Transition*; Murphy, O. J., Ed.; Plenum Press: New York, 1992; pp 359−369.
(24) Ross, P. N. *Electrochim. Acta* **1991**, *36*, 2053−2062.
(25) Leger, J. M.; Lamy, C. *Ber. Bunsen-Ges. Chem.* **1990**, *94*, 1021−1025.
(26) Beden, B.; Kadirgan, F.; Lamy, C.; Leger, J. M. *J. Electroanal. Chem. Interfacial Electrochem.* **1981**, *127*, 75−85.
(27) Wasmus, S.; Kuver, A. *J. Electroanal. Chem.* **1999**, *461*, 14−31.
(28) Hogarth, M. P.; Hards, G. A. *Platinum Met. Rev.* **1996**, *40*, 150−159.
(29) Frelink, T.; Visscher, W.; Vanveen, J. A. R. *Electrochim. Acta* **1994**, *39*, 1871−1875.
(30) Park, K. W.; Choi, J. H.; Kwon, B. K.; Lee, S. A.; Sung, Y. E.; Ha, H. Y.; Hong, S. A.; Kim, H.; Wieckowski, A. *J. Phys. Chem. B* **2002**, *106*, 1869−1877.
(31) Choi, J.-H.; Park, K.-W.; Park, I.-S.; Nam, W.-H.; Sung, Y.-E. *Electrochim. Acta* **2004**, *50*, 787−790.
(32) Ley, K. L.; Liu, R. X.; Pu, C.; Fan, Q. B.; Leyarovska, N.; Segre, C.; Smotkin, E. S. *J. Electrochem. Soc.* **1997**, *144*, 1543−1548.

10.1021/om0610750 CCC: $37.00
Publication on Web 05/18/2007

Surface studies on Pt anodes showed that Pt is poisoned by adsorbed CO, which is formed as an intermediate during the electrooxidation process.[33−35] Addition of a second metal improved the anode behavior, with RuPt[26,36−39] systems proving to be particularly effective. In the "bifunctional mechanism" initially proposed by Watanabe and Motoo,[40] the Pt sites are responsible for the binding and dehydrogenation of methanol, while the Ru sites activate water through formation of Ru−oxo intermediates, which are involved in the conversion of surface-bound CO to CO_2.

Cooperative interactions in heterobinuclear systems have been the primary target in the development of our catalysts for the electrooxidation of alcohols and led us to prepare the heterobimetallic complexes $Cp(PPh_3)Ru(\mu\text{-}Cl)(\mu\text{-}dppm)PtCl_2$ (**1**),[41] $Cp(PPh_3)Ru(\mu\text{-}Cl)(\mu\text{-}dppm)PdCl_2$ (**2**),[42] and $Cp(PPh_3)RuCl(\mu\text{-}dppm)AuCl$ (**3**).[42] These complexes were found to be effective catalysts for electrooxidation of methanol, resulting in much higher current efficiencies in comparison with those obtained with the model compound $CpRu(PPh_3)_2Cl$.[43] Clearly, the enhancement of the catalytic activity is due to the presence of the second metal. As a continuation of our work, the replacement of ruthenium by its congener iron was investigated. Catalysis by iron complexes has been of recent interest, due to their reactivity and the possibility of replacing expensive precious metals with the more readily available first-row metals.[44−52] We now report the synthesis and characterization of new carbonyl-containing Ru/Pt, Ru/Pd, and Ru/Au derivatives of **1**−**3**, as well as their isoelectronic Fe/Pt, Fe/Pd, and Fe/Au analogues. X-ray crystallography, cyclic voltammetry, and IR, UV−vis, and NMR (^1H and ^{31}P) spectroscopy were used to examine the electronic interaction between the two metal centers.

Experimental Section

General Procedures. All reactions and manipulations were performed under an argon atmosphere using standard Schlenk techniques. Pentane and ethyl ether were dried by distillation from Na/Ph_2CO. Acetonitrile and 1,2-dichloroethane were dried by distillation from CaH_2. Benzene and dichloromethane were dried with an MBraun solvent purification system. All solvents were saturated with argon prior to use. All deuterated solvents for NMR measurements (Cambridge Isotope Laboratories) were degassed via freeze−pump−thaw cycles and stored over molecular sieves (4 Å). ^1H and $^{31}P\{^1H\}$ NMR spectra were recorded at room temperature on a Varian Mercury 300 spectrometer operating at 300 and 121 MHz, respectively, with chemical shifts (δ, ppm) reported relative to tetramethylsilane (^1H NMR) or 85% H_3PO_4 (^{31}P NMR). IR spectra were obtained as neat films on NaCl using a Perkin-Elmer Spectrum One FT-IR spectrophotometer. UV−vis spectra were recorded on a Shimadzu UV-1650PC spectrophotometer using silica quartz cells (1 cm path length). Elemental analyses (C, H) were performed by Robertson Microlit Laboratories, Madison, NJ. $CpRu(PPh_3)(\mu\text{-}I)(\mu\text{-}dppm)PtI_2$ (**12**),[53] $CpRu(PPh_3)I(\kappa^1\text{-}dppm)$ (**17**),[53] $CpRu(PPh_3)I(\mu\text{-}dppm)AuI$ (**16**),[53] $CpFe(CO)(\kappa^1\text{-}dppm)I$ (**7**),[54] $CpRu(PPh_3)(CO)I$ (**4**),[55] $CpFe(PPh_3)(CO)I$ (**5**),[56] PPh_3AuI (**18**),[57] and $CpRu(CO)_2I$[58] were prepared as previously described. All other starting materials were purchased in reagent-grade purity and used without further purification.

Electrochemical experiments were performed at ambient temperature in a glovebox using an EG&G PAR Model 263A potentiostat/galvanostat. Cyclic voltammograms (CV) were recorded in 3.5 mL of DCE/0.1 M tetrabutylammonium hexafluorophosphate (TBAH) or tetrabutylammonium triflate (TBAT) at ambient temperature under nitrogen. All potentials are reported versus NHE and referenced to Ag/Ag^+. The reference electrode consisted of a silver wire immersed in an acetonitrile solution containing freshly prepared 0.01 M $AgNO_3$ and 0.1 M TBAH or TBAT. The Ag^+ solution and silver wire were contained in a 75 mm glass tube fitted at the bottom with a Vycor tip. Cyclic voltammetry was performed in a three-compartment H-cell separated by a medium-porosity sintered-glass frit in 2.5−3.5 mL of DCE/0.1 M TBAH or TBAT at room temperature under nitrogen. A glassy-carbon electrode (diameter 3 mm) was the working electrode, and a platinum flag was used as the counter electrode. All electrochemical measurements were performed inside the glovebox. The $E°$ values for the ferrocenium/ferrocene couple in DCE/0.1 M TBAH and DCE/0.1 M TBAT were +0.67 and +0.68 V.

$CpRu(CO)(\kappa^1\text{-}dppm)I$ (6). In a Schlenk flask a solution of $CpRu(CO)_2I$ (1.08 g, 3.10 mmol) and dppm (1.25 g, 3.25 mmol) in 150 mL of benzene was refluxed for 12 h. The solvent was removed under vacuum. Purification of the product was achieved by column chromatography on silica gel using CH_2Cl_2 as eluent to afford 1.53 g (70.1%) of **6** as an orange powder. Anal. Calcd for $C_{31}H_{27}IOP_2Ru$: C, 52.78; H, 3.86. Found: C, 53.04; H, 3.78.

$CpRu(CO)(\mu\text{-}I)(\mu\text{-}dppm)PtI_2$ (8). A solution of **6** (0.400 g, 0.567 mmol) in CH_2Cl_2 (15 mL) was added to a suspension of $Pt(COD)I_2$ (0.347 g, 0.625 mmol) in CH_2Cl_2 (5 mL). The resulting solution was stirred for 1 h at ambient temperature. The solvent was removed under vacuum, and purification was achieved by column chromatography on silica gel using CH_2Cl_2 as eluent.

(33) Wasmus, S.; Vielstich, W. *J. Appl. Electrochem.* **1993**, *23*, 120−124.
(34) Hamnett, A.; Weeks, S. A.; Kennedy, B. J.; Troughton, G.; Christensen, P. A. *Ber. Bunsen-Ges. Chem.* **1990**, *94*, 1014−1020.
(35) Pathanjali, G. A.; Chireau, R. F. *Bull. Electrochem.* **1991**, *7*, 497−499.
(36) Gasteiger, H. A.; Markovic, N.; Ross, P. N.; Cairns, E. J. *J. Phys. Chem.* **1993**, *97*, 12020−12029.
(37) Goodenough, J. B.; Hamnett, A.; Kennedy, B. J.; Manoharan, R.; Weeks, S. A. *J. Electroanal. Chem. Interfacial Electrochem.* **1988**, *240*, 133−145.
(38) Swathirajan, S.; Mikhail, Y. M. *J. Electrochem. Soc.* **1991**, *138*, 1321−1326.
(39) Watanabe, M.; Uchida, M.; Motoo, S. *J. Electroanal. Chem. Interfacial Electrochem.* **1987**, *229*, 395−406.
(40) Watanabe, M.; Motoo, S. *J. Electroanal. Chem. Interfacial Electrochem.* **1975**, *60*, 276−283.
(41) Tess, M. E.; Hill, P. L.; Torraca, K. E.; Kerr, M. E.; Abboud, K. A.; McElwee-White, L. *Inorg. Chem.* **2000**, *39*, 3942−3944.
(42) Matare, G.; Tess, M. E.; Abboud, K. A.; Yang, Y.; McElwee-White, L. *Organometallics* **2002**, *21*, 711−716.
(43) Anthony, C. R.; McElwee-White, L. *J. Mol. Catal. A: Chem.* **2005**, *227*, 113−117.
(44) Small, B. L.; Brookhart, M. *Macromolecules* **1999**, *32*, 2120−2130.
(45) Britovsek, G. J. P.; Bruce, M.; Gibson, V. C.; Kimberley, B. S.; Maddox, P. J.; Mastroianni, S.; McTavish, S. J.; Redshaw, C.; Solan, G. A.; Stromberg, S.; White, A. J. P.; Williams, D. J. *J. Am. Chem. Soc.* **1999**, *121*, 8728−8740.
(46) Bianchini, C.; Mantovani, G.; Meli, A.; Migliacci, F.; Zanobini, F.; Laschi, F.; Sommazzi, A. *Eur. J. Inorg. Chem.* **2003**, 1620−1631.
(47) Bolm, C.; Legros, J.; Le Paih, J.; Zani, L. *Chem. Rev.* **2004**, *104*, 6217−6254.
(48) Bianchini, C.; Giambastiani, G.; Guerrero, I. R.; Meli, A.; Passaglia, E.; Gragnoli, T. *Organometallics* **2004**, *23*, 6087−6089.
(49) Sun, W. H.; Tang, X. B.; Gao, T. L.; Wu, B.; Zhang, W. J.; Ma, H. W. *Organometallics* **2004**, *23*, 5037−5047.
(50) MacKay, B. A.; Fryzuk, M. D. *Chem. Rev.* **2004**, *104*, 385−401.
(51) Bart, S. C.; Lobkovsky, E.; Bill, E.; Chirik, P. J. *J. Am. Chem. Soc.* **2006**, *128*, 5302−5303.
(52) Bart, S. C.; Lobkovsky, E.; Chirik, P. J. *J. Am. Chem. Soc.* **2004**, *126*, 13794−13807.
(53) Yang, Y.; Abboud, K. A.; McElwee-White, L. *Dalton Trans.* **2003**, 4288−4296.
(54) Haines, R. J.; DuPreez, A. L. *Inorg. Chem.* **1972**, *11*, 330−336.
(55) Brown, D. A.; Lyons, H. J.; Sane, R. T. *Inorg. Chim. Acta* **1970**, *4*, 621−625.
(56) Coville, N. J.; Darling, E. A.; Hearn, A. W.; Johnston, P. *J. Organomet. Chem.* **1987**, *328*, 375−385.
(57) Barron, P. F.; Engelhardt, L. M.; Healy, P. C.; Oddy, J.; White, A. H. *Aust. J. Chem.* **1987**, *40*, 1545−1555.
(58) Haines, R. J.; DuPreez, A. L. *J. Chem. Soc., Dalton Trans.* **1972**, 944−948.

Scheme 1. Synthetic Routes to the Heterobimetallic Complexes

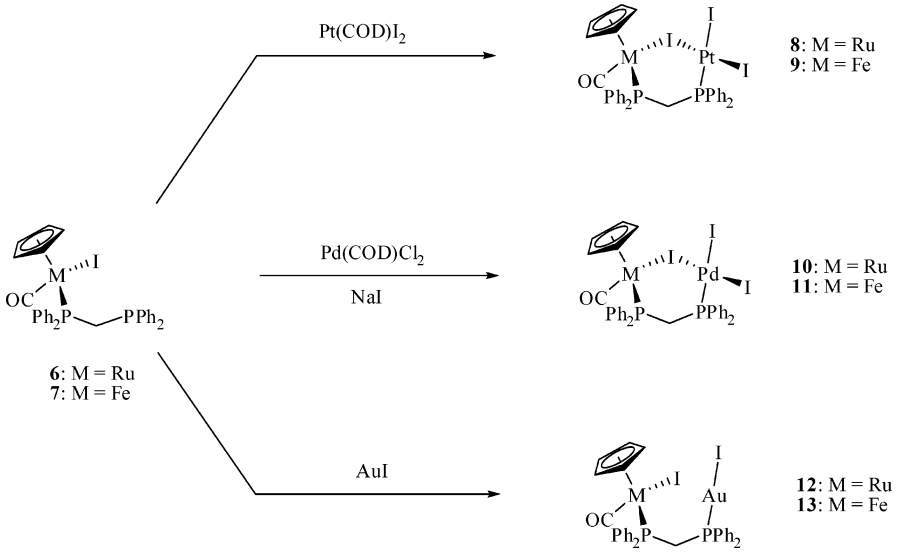

Chart 1

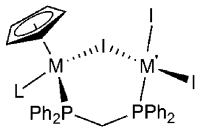

Complex	M	M′	L
8	Ru	Pt	CO
9	Fe	Pt	CO
10	Ru	Pd	CO
11	Fe	Pd	CO
14	Ru	Pt	PPh_3
15	Ru	Pd	PPh_3

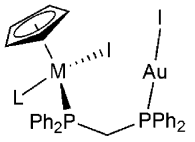

Complex	M	L
12	Ru	CO
13	Fe	CO
16	Ru	PPh_3

Yield: 0.37 g, 57.6%. Anal. Calcd for $C_{31}H_{27}I_3OP_2PtRu$: C, 32.25; H, 2.36. Found: C, 32.28; H, 2.26.

CpFe(CO)(μ-I)(μ-dppm)PtI_2 (9). Using the same procedure as for **8**, a solution of CpFe(CO)(κ^1-dppm)I (0.500 g, 0.756 mmol) and Pt(COD)I_2 (0.463 g, 0.831 mmol) in 20 mL of CH_2Cl_2 was stirred for 1 h at ambient temperature. After purification, **9** was obtained as a pale green solid. Yield: 0.493 g, 62.3%. Anal. Calcd for $C_{31}H_{27}FeI_3OP_2Pt$: C, 33.57; H, 2.45. Found: C, 33.50; H, 2.44.

CpRu(CO)(μ-I)(μ-dppm)PdI_2 (10). To a solution of **6** (0.400 g, 0.567 mmol) in CH_2Cl_2 (20 mL) was added a solution of Pd(COD)Cl_2 (0.178 g, 0.623 mmol) in CH_2Cl_2 (20 mL). After the mixture was stirred for 1 h at ambient temperature, 10 equiv of NaI (0.85 g, 5.67 mmol) was added and the resulting suspension was stirred for 24 h. After evaporation of the solvent under vacuum, purification was achieved by column chromatography on silica gel (CH_2Cl_2) to give **10** as a dark brown powder. Yield: 0.503 g, 83.2%. Anal. Calcd for $C_{31}H_{27}I_3OP_2PdRu$: C, 34.94; H, 2.55. Found: C, 34.76; H, 2.34.

CpFe(CO)(μ-I)(μ-dppm)PdI_2 (11). A solution of CpFe(CO)(κ^1-dppm)I (0.200 g, 0.303 mmol), Pd(COD)Cl_2 (0.103 g, 0.303 mmol), and NaI (0.450 g, 3.03 mmol) in 50 mL of CH_2Cl_2 was reacted in a manner similar to that described above for **10.** Similar purification afforded **11** as a dark brown solid. Yield: 0.203 g, 65.6%. Anal. Calcd for $C_{31}H_{27}FeI_3OP_2Pd$: C, 36.49; H, 2.67. Found: C, 36.56; H, 2.31.

CpRu(CO)I(μ-dppm)AuI (12). A solution of **6** (0.25 g, 0.36 mmol) in CH_2Cl_2 (15 mL) was added at −20 °C to a solution of AuI (0.11 g, 0.36 mmol) in CH_2Cl_2 (15 mL). The reaction mixture was stirred for 1 h at ambient temperature, and after evaporation of the solvent, purification was achieved by extraction with approximately 30 mL of ethyl ether, leading to **12** as an orange solid. Yield: 0.29 g, 78.5%. Anal. Calcd for $C_{31}H_{27}AuI_2OP_2Ru$: C, 36.17; H, 2.64. Found: C, 36.20; H, 2.45.

CpFe(CO)I(μ-dppm)AuI (13). In the same manner described for **12,** a solution of **7** (0.70 g, 10.6 mmol) and AuI (0.40 g, 10.6 mmol) in CH_2Cl_2 (50 mL) was stirred for 1 h. After evaporation of the solvent, purification was achieved by column chromatography on silica gel using CH_2Cl_2 as eluent to afford **13** as a dark green solid. Yield: 0.67 g, 64.3%. Anal. Calcd for $C_{31}H_{27}AuFeI_2OP_2$: C, 37.83; H, 2.77. Found: C, 37.53; H, 2.57.

CpRu(PPh_3)(μ-I)(μ-dppm)PdI_2 (15). A solution of CpRu(PPh_3)(κ^1-dppm)I (**17**; 0.40 g, 0.43 mmol), Pd(COD)Cl_2 (0.13 g, 0.45 mmol), and NaI (0.32 g, 2.16 mmol) in 50 mL of CH_2Cl_2 was reacted in a manner similar to that described above for **10**. After evaporation of the solvent, the purification was achieved by recrystallization from dichloromethane/pentane to yield **15** as a dark brown powder. Yield: 0.35 g, 63.5%. ^{1}H NMR ($CDCl_3$): δ 8.09−5.81 (m, 35H, C_6H_5), 4.62 (s, 5H, C_5H_5), 3.49 (m, 1H, PCH_2P), 2.94 (m, 1H, (PCH_2P)). ^{31}P{^{1}H} NMR ($CDCl_3$): δ 48.23 (dd, Ru−PPh$_2$, J_{PP} = 35.4, 20.7 Hz), 40.40 (dd, Ru−PPh$_3$, J_{PP} = 35.4, 6.7 Hz), 12.7 (dd, Pd−PPh$_2$, J_{PP} = 20.7, 6.7 Hz). HRMS (FAB): *m*/*z* calcd for $C_{48}H_{42}I_2P_3PdRu$, 1172.8667 $(M-I)^{\bullet+}$; found, 1172.8758.

Results and Discussion

Synthesis of Complexes 6 and 7. Details of the preparation and spectroscopic data for CpFe(CO)(κ^1-dppm)I (**7**) have been reported.[54] The ruthenium analogue was synthesized by following a similar procedure. Reaction of $CpRu(CO)_2I$ with dppm in refluxing benzene afforded CpRu(CO)(κ^1-dppm)I (**6**) in greater than 70% yield.

Synthesis of Heterobimetallic Complexes 8−13. Reactions of CpRu(CO)(κ^1-dppm)I (**6**) or CpFe(CO)(κ^1-dppm)I (**7**) with Pt(COD)I_2 in CH_2Cl_2 afford the I-bridged Ru/Pt complex **8** (57% yield) and Fe/Pt complex **9** (62% yield), respectively (Scheme 1; see also Chart 1). During the reactions, small amounts of Pt(κ^2-dppm)I_2 were formed by dppm transfer to Pt(COD)I_2. This byproduct can be detected by ^{31}P NMR as a singlet with Pt satellites at ca. −70 ppm. Complexes **8** and **9** were obtained as a bright orange solid and a pale green solid, respectively. These

Table 1. Selected NMR (^{1}H, ^{31}P{^{1}H}) and IR Data for Complexes 4−13

	^{1}H NMR (δ)[a]		^{31}P NMR (δ)[a]			
	Cp	−CH_2−	Ru−PPh_2−	Fe−PPh_2−	M−PPh_2	IR (cm^{-1})[b] $\nu_{CO'}$
4	4.92		49.87 (s)			1950
5	4.42			68.44 (s)		1941
6	4.85	3.81−3.56 (m)	44.3 (d)		−23.8 (d)	1952
7	4.38	3.59 (m), 3.16 (m)		63.3 (d)	−24.0 (d)	1946
8	5.02	4.10 (m), 3.73 (m)	43.5 (d)		−3.3 (d)	1969
9	4.51	3.72 (m)		65.3 (d)	−4.3 (d)	1963
10	5.07	4.01 (m), 3.64 (m)	46.7 (d)		12.6 (d)	1968
11	4.56	3.72 (m), 3.44 (m)		69.2 (d)	12.2 (d)	1960
12	4.82	4.70 (m), 3.63 (m)	40.6 (d)		26.9 (d)	1952
13	4.36	4.46 (m), 3.19 (m)		62.0 (d)	27.6 (d)	1945

[a] Spectra measured in $CDCl_3$, at room temperature. [b] Neat film.

complexes are moderately stable in the solid state but decompose slowly in solution if stored outside a glovebox. Since Pd(COD)-I_2 could not be isolated, the I-bridged Ru/Pd complex **10** (83% yield) and Fe/Pd complex **11** (65% yield) were prepared by reacting **6** and **7** with Pd(COD)Cl_2 in CH_2Cl_2, followed by treatment with 10 equiv of NaI. The Ru/Au complex **12** (78% yield) and Fe/Au complex **13** (64% yield), in which the two metal centers are linked only via the dppm bridge, were prepared by direct reaction of **6** and **7** with AuI. Although pure samples of the Ru/Au complex **12** could be isolated, it was found to be the most sensitive of the heterobimetallic complexes. Degradation of **12** could be observed in the solid state even when it was stored under nitrogen.

Synthesis of Complex 15. The heterobimetallic Ru/Pd complex **15** was prepared in a manner similar to that for **10** and obtained as a dark brown solid (63%). The stability of complex **15** was also found to be similar to those of other I-bridged complexes synthesized in this work.

NMR Data. The ^{31}P NMR spectra of the iron complexes **9**, **11**, and **13** showed features for the phosphine ligands similar to those previously reported for CpFe(CO)(μ-I)(μ-dppm)M(CO)$_4$ (M = Cr, Mo, W).[59] A pair of doublets is always observed, with the downfield resonance corresponding to the Fe-bound phosphorus, while the upfield doublet is assigned to phosphorus coordinated to the second metal (Pt, Pd, or Au). The spectra of the ruthenium complexes **8**, **10**, and **12** are similar and can be assigned in an analogous fashion. Chemical shifts (δ) as well as coupling constants are reported in Table 1.

It has been noted that for metal phosphine complexes of the same structure and oxidation state, one generally observes a shift of the ^{31}P resonance to higher field as one descends in a given group.[60] Accordingly, we clearly see a decrease in δ_P as one descends from Fe to Ru. Interaction between Fe or Ru and the second metal can be detected by careful examination of the M-bound phosphorus (M = Fe, Ru). We also see a decrease in δ_P for the Fe-bound phosphorus from 69.2 to 65.3 ppm as one descends from Pd to Pt in complexes **11** and **9**, respectively. Variation in δ_P also follows this trend for the Ru series. When the M′-bound (M′ = Pt, Pd) phosphorus shifts are compared, we can clearly see a decrease in δ_P for the Ru-bound phosphorus from 46.7 to 43.5 ppm when the metal goes from Pd to Pt for compounds **10** and **8**, respectively. Although a similar trend in the phosphorus shifts from Fe (62.0 ppm) to Ru (40.6 ppm) can be observed for the Ru/Au and Fe/Au complexes **12** and **13**, no further comparison with the I-bridged compounds can be made, due to the differences in structures and oxidation states compared to those for the I-bridged complexes.

Table 2. Crystal Data and Structure Refinement Details for Complexes 8 and 9

	8	**9**
empirical formula	$C_{33}H_{31}Cl_2I_3O$-P_2PtRu	$C_{33}H_{31}Cl_2I_3O$-P_2PtFe
M_r	1253.28	1278.96
T/K	173(2)	173(2)
λ/Å	0.710 73	0.710 73
cryst syst	monoclinic	monoclinic
space group	$P2_12_12_1$	$P2_12_12_1$
a/Å	11.8206(8)	13.7053(9)
b/Å	12.9648(9)	14.9673(9)
c/Å	24.4701(17)	18.7364(12)
α/deg	90	90
β/deg	90	99.6020(10)
γ/deg	90	90
V/Å^3	3750.1(4)	3789.6(4)
Z	4	4
D_c/Mg m^{-3}	2.220	2.242
μ/mm^{-1}	6.852	6.908
F_{000}	2328	2392
cryst size/mm	0.28 × 0.21 × 0.10	0.18 × 0.09 × 0.03
θ range/deg	1.66−27.50	1.71−27.50
index ranges	$-13 \le h \le 15$ $-14 \le k \le 16$ $-28 \le l \le 31$	$-17 \le h \le 15$ $-19 \le k \le 12$ $-20 \le l \le 24$
no. of rflns collected	22 870	24 440
no. of indep rflns (R_{int})	8433 (0.0462)	8580 (0.0909)
completeness to θ = 27.49°/%	99.4	98.4
abs cor	integration	integration
max/min transmissn	0.5224/0.2130	0.8179/0.3668
no. of data/restraints/params	8433/0/399	8580/0/352
GOF on F^2 [a]	1.054	0.899
R1[b]	0.0264	0.0732
wR2[c]	0.0587	0.1035
largest diff peak, hole/e Å^{-3}	1.134, −1.043	2.911, −1.983

[a] GOF = $S = [w(F_o^2 - F_c^2)^2]/(n-p)]^{1/2}$; $w = 1/[\sigma^2(F_o^2) + 0.0337p)^2 + 1.24p]$; $p = [\max(F_o^2, 0) + 2F_c^2]/3$. [b] R1 = $\sum(||F_o| - |F_c||)/\sum|F_o|$. [c] wR2 = $[\sum[w(F_o^2 - F_c^2)^2]/\sum[w(F_o^2)^2]^{1/2}$.

Selected ^{1}H NMR data for **4**−**13** are reported in Table 1. The spectra for the iron complexes **9**, **11**, and **13** exhibit chemical shift values similar to those previously published.[59] A sharp singlet in the range 4.36−4.51 ppm is observed for the Cp protons, and the diastereotopic methylene protons of the bridging dppm appear as two sets of doublet of doublet of doublets centered in the range 3.19−4.46 ppm as a result of the coupling to each other and to the two adjacent phosphorus atoms. The spectra for the ruthenium analogues **8**, **10**, and **12** are similar, with a sharp singlet for the Cp protons observed in the range 4.82−5.07 ppm and the two sets of multiplets for the diastereotopic methylene protons centered in the range 3.63−4.70 ppm.

IR Spectroscopy. The IR data for compounds **4**−**13** are reported in Table 1. The infrared spectra of all the complexes displayed a single carbonyl stretching frequency in the range 1945−1969 cm^{-1}, characteristic of terminal CO ligands. Examination of ν_{CO} provides a powerful tool to explore the electronic interactions in the bimetallic complexes. As electron donation from metal d orbitals to π^*_{CO} increases, there is a concomitant decrease in ν_{CO}. On this basis, the infrared data are consistent with an increase of the electron density at the carbonyl along the following compound series: Ru/Pt (**8**) ≈ Ru/Pd (**10**) < Fe/Pt (**9**) < Fe/Pd (**11**) < Ru monomer (**4**) ≈ Ru monomer (**6**) ≈ Ru/Au (**12**) < Fe/Au (**11**) ≈ Fe monomer (**5**) ≈ Fe monomer (**7**). A possible explanation for

(59) Hsu, M.-A.; Yeh, W.-Y.; Chiang, M. Y. *J. Organomet. Chem.* **1998**, *552*, 135−143.
(60) Garrou, P. E. *Chem. Rev.* **1981**, *81*, 229−266.

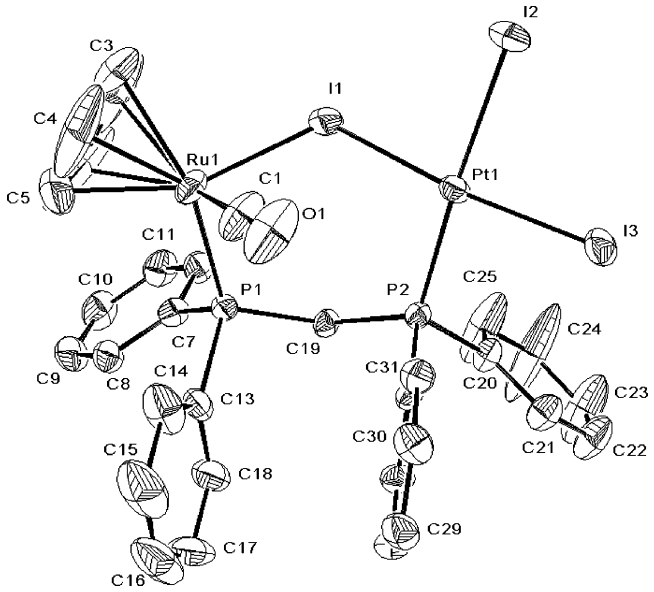

Figure 1. ORTEP drawing of the molecular structure of Cp(CO)-Ru(μ-I)(μ-dppm)PtI_2 (**8**). Thermal ellipsoids are plotted at the 50% probability level. Hydrogen atoms are omitted for clarity.

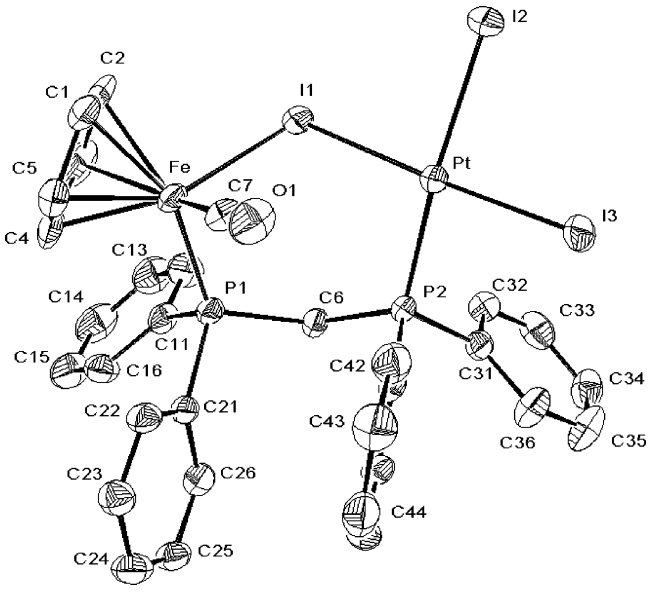

Figure 2. ORTEP drawing of the molecular structure of Cp(CO)-Fe(μ-I)(μ-dppm)PtI_2 (**9**). Thermal ellipsoids are plotted at the 50% probability level. Hydrogen atoms are omitted for clarity.

the tendencies in the bridged complexes is that the two metals communicate inductively through the σ bonds of the iodide bridge. This would be consistent with the bridging iodide being an important conduit for the shifts in electronic density from the Ru or Fe center to Pd or Pt that are observed in complexes **8**−**11**. On the other hand, the values of ν_{CO} for the Ru/Au and Fe/Au complexes **12** and **13**, which are bridged only by dppm, are nearly identical with those of the corresponding mononuclear Ru and Fe complexes **4**−**7**. This is consistent with limited interactions between the Ru or Fe and Au through the dppm bridge.

X-ray Crystallography. X-ray structures were obtained for the I-bridged complexes **8**−**11**. Crystallographic details for the Ru/Pt complex **8** and the Fe/Pt complex **9** are provided in Table 2. Crystallographic details for the Ru/Pd complex **10** and the Fe/Pd complex **11** are available in the Supporting Information. All of these complexes show structures similar to those of I-bridged complexes previously reported,[42,53,59] where the coordination about the iron and ruthenium atoms retained a piano-stool configuration and the coordination about the Pt and Pd atoms is distorted square planar.

Shown in Figures 1 and 2 are the ORTEP drawings of the Ru/Pt and Fe/Pt compounds **8** and **9**, respectively. Selected bond distances and bond angles for compounds **8** and **9** appear in Tables 3 and 4, respectively. Structural data for the Ru/Pd complex **10** and the Fe/Pd complex **11** are available in the Supporting Information. In each complex, the two metals are linked by the dppm ligand and iodine atom to form a distorted six-membered ring. Consistent with the IR data, the carbonyl ligands for **8**−**11** are terminal. As previously noted for heterobimetallic iron complexes,[59] the cyclopentadienyl ring is bound asymmetrically to Ru or Fe, with the Ru−C(Cp) distances ranging from 2.168(7) to 2.248(8) Å, while the Fe−C(Cp) distances range from 2.071(8) to 2.102(8) Å. The shortest metal−carbon bond lengths (Ru1−C5 and Fe-C5) are due to the trans influence from the iodide ligand (C5−Ru1−I1 = 148° and C5−Fe−I1 = 150°). The M−I−M′ angles and bond distances in **8**−**11** fall within the range of expected values,[61] with asymmetric M−I and M′−I distances varying between 2.5944(4) and 2.6962(5) Å. The Ru−I distance for **8**, 2.6620(6) Å, is comparable to the value of 2.6749(5) Å reported previously for the related complex $CpRu(PPh_3)(\mu\text{-I})(\mu\text{-dppm})PdCl_2$.[41]

Table 3. Selected Bond Distances (Å) and Angles (deg) for CpRu(CO)(μ-I)(μ-dppm)PtI_2 (8)

Ru1−I1	2.6620(6)	Ru1−C3	2.227(7)
Pt1−I1	2.5944(4)	Ru1−C4	2.168(7)
C1−O1	1.147(7)	Ru1−C5	2.156(10)
Ru1−C1	1.864(6)	Ru1−C6	2.190(10)
Ru1−C2	2.248(8)		
Pt1−I1−Ru1	108.233(15)	O1−C1−Ru1	174.6(5)
I1−Pt1−I3	173.163(12)	C5−Ru1−I1	148.6(4)
I1−Pt1−I2	88.38(9)		

Table 4. Selected Bond Distances (Å) and Angles (deg) for CpFe(CO)(μ-I)(μ-dppm)PtI_2 (9)

Fe−I1	2.6001(12)	Fe−C2	2.100(7)
Pt−I1	2.6071(5)	Fe−C3	2.088(6)
C7−O1	1.138(8)	Fe−C4	2.073(7)
Fe−C7	1.783(8)	Fe−C5	2.071(8)
Fe−C1	2.102(8)		
Fe−I1-Pt	108.46(3)	O1−C7−Fe	173.3(7)
I1−Pt−I3	176.86(2)	C5−Fe−I1	150.1(2)
I1−Pt−I2	87.399(17)		

Cyclic Voltammetry. Cyclic voltammetry was performed on heterobimetallic complexes **8**−**13** as well as the monometallic complexes **4** and **5**. The monometallic complexes CpRu(CO)-(κ^1-dppm)I (**6**) and CpFe(CO)(κ^1-dppm)I (**7**) were not used for comparison, since after multiple CV cycles for **6** or **7**, a new oxidation wave at the redox potential of the substitution product Cp$M(\kappa^2$-dppm)I grows in. In addition to these complexes, electrochemical experiments were also carried out with ruthenium triphenylphosphine complexes **14** and **16**,[53] as well as with the Ru/Pd complex **15**, which was prepared for comparison purposes. The CV data for complexes **4**, **5**, **8**−**16**, and **18** are given in Table 5, while representative cyclic voltammograms of complexes **5**, **8**, and **13** are provided in Figures 3−5, respectively. The cyclic voltammograms for the heterobimetallic complexes **8**−**13** each display three waves in the 1.00−2.27 V range (e.g., Figures 4 and 5). These redox processes have been

(61) Blake, A. J.; Lippolis, V.; Parsons, S.; Schröder, M. *J. Chem. Soc., Chem. Commun.* **1996**, 2207−2209.

Table 5. Formal Potentials for Complexes 4−17[a]

complex	couple	$E_{p,a}$/V	$E_{1/2}$[b]/V	couple	$E_{p,a}$/V	$E_{1/2}$[b]/V	couple	$E_{p,a}$/V	ref
Fc/Fc^+	Fe(II/III)	0.76	0.67						*i*
4	Ru(II/III)	1.15					Ru(III/IV)	1.93	*i*
5	Fe(II/III)	0.95	0.88				Fe(III/IV)	2.18	*i*
8	Ru(II/III)	0.96		Pt(II/IV)	1.85	1.76	Ru(III/IV)	2.00	*i*
9	Fe(II/III)	0.97		Pt(II/IV)	1.54	1.48	Fe(III/IV)	2.20	*i*
14[c,d,h]	Ru(II/III)	1.10		Pt(II/IV)	1.49	1.43	Ru(III/IV)	1.98	53
10	Ru(II/III)	0.90		Pd(II/IV)	1.87	1.79	Ru(III/IV)	1.99	*i*
11	Fe(II/III)	0.95		Pd(II/IV)	1.57	1.51	Fe(III/IV)	2.27	*i*
15[c,e,h]	Ru(II/III)	1.29		Pd(II/IV)	1.55	1.50	Ru(III/IV)	1.98	*i*
12	Ru(II/III)	0.99		Au(I/III)	1.78	1.72	Ru(III/IV)	2.02	*i*
13[c]	Fe(II/III)	0.99	0.92	Au(I/III)	1.61	1.49	Fe(III/IV)	1.99	*i*
16[c,f,h]	Ru(II/III)	0.97	0.89	Au(I/III)	1.54		Ru(III/IV)	1.80	53
18[c,g,h]				Au(I/III)	1.62				*i*

[a] All potentials obtained in 0.1 M DCE/TBAH (tetrabutylammonium hexafluorophosphate) unless otherwise specified and reported vs NHE. $\nu = 10$ mV/s. [b] $E_{1/2}$ reported for reversible waves. [c] Potentials obtained in 0.1 M DCE/TBAT (tetrabutylammonium triflate). [d] $CpRu(PPh_3)(\mu\text{-}I)(\mu\text{-dppm})PtI_2$. [e] $CpRu(PPh_3)(\mu\text{-}I)(\mu\text{-dppm})PdI_2$. [f] $CpRu(PPh_3)I(\mu\text{-dppm})AuI$. [g] PPh_3AuI. [h] $\nu = 50$ mV/s. [i] This work.

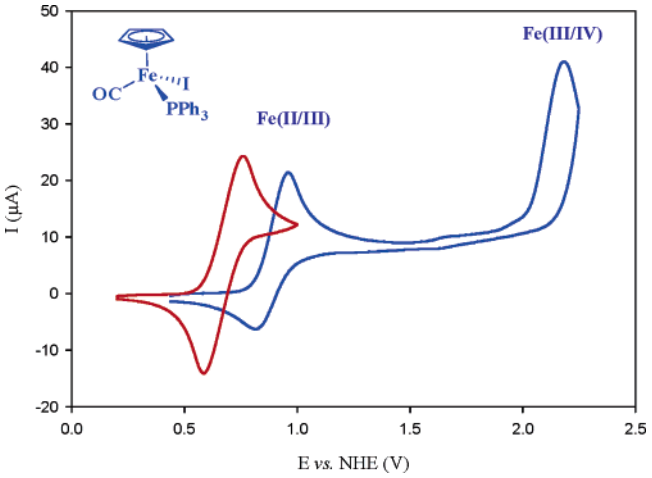

Figure 3. Cyclic voltammograms of complex **5** (5 mM; blue line) and ferrocene (5 mM; red line) in DCE/0.1 M TBAH at a scan rate of 10 mV/s.

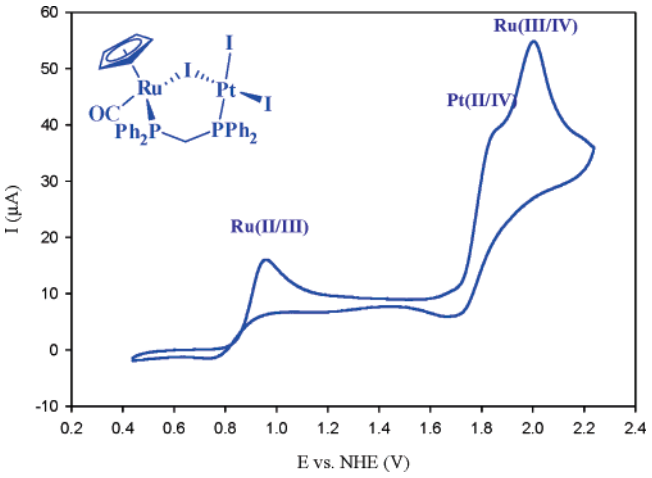

Figure 4. Cyclic voltammogram of complex **8** (5 mM) in DCE/0.1 M TBAH at a scan rate of 10 mV/s.

previously described for several Ru heterobimetallic complexes having similar structures.[41,42,53] For the ruthenium complexes **8**, **10**, and **12**, the first and third waves are assigned to the Ru(II/III) and Ru(III/IV) couples, respectively, while the second wave is assigned to the redox couple of the second metal. For iron complexes **9**, **11**, and **13**, the trend is very similar to that for the ruthenium analogue, with the first and third waves assigned to the Fe(II/III) and Fe(III/IV) couples, respectively, and the middle one assigned to the redox couple of the second

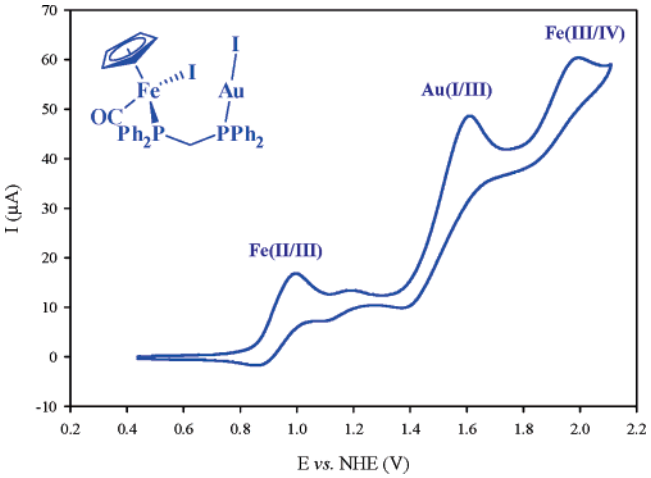

Figure 5. Cyclic voltammogram of complex **13** (5 mM) in DCE/0.1 M TBAT at a scan rate of 10 mV/s.

metal. The irreversibility of some of the oxidation waves is consistent with a chemical reaction following oxidation. Whether this is ligand loss/exchange or dissociation into monometallic species is not yet clear.

Electronic interactions between the two metals in the I-bridged heterobimetallic complexes **8**−**11** are evidenced by the differences in redox potential of the second metal (Pt, Pd, or Au) when a Ru complex is compared to its Fe analogue. These differences are significantly greater when the two metals are bridged by both iodide and dppm (cf. **8** and **9**, or **10** and **12**) than they are with only the dppm bridge (**12** and **13**). The cyclic voltammograms of the Ru/Pt complex **8** and the Fe/Pt complex **9** exhibit irreversible oxidation waves at 0.96 V vs NHE for **8**, assigned to Ru(II/III), and at 0.97 V for the Fe(II/III) couple of **9**. The Ru/Pt complex **8** exhibits a second quasi-reversible wave at 1.76 V assigned to the Pt(II/IV) couple, overlapping with an irreversible oxidation wave at 2.00 V assigned to the Ru(III/IV) couple. For the Fe/Pt analogue **9**, the quasi-reversible Pt(II/IV) wave is shifted negatively about 280 mV ($E_{1/2} = 1.48$ V) in comparison to the analogous wave from complex **8**. This shift is evidence of a more significant electron donation from Fe to Pt through the I bridge in Fe/Pt complex **9** in comparison to its Ru/Pt analogue **8**. The carbonyl stretching frequencies for complexes **8** and **9** differ by 6 cm^{-1}, which is roughly the difference between ν_{CO}(Ru) and ν_{CO}(Fe) for all the congeneric pairs of complexes, including monomers **4**−**7**. A similar difference (about 10 cm^{-1}) has also been reported for the terminal carbonyls in the heterobimetallic complexes MCl(CO)-

(μ-CO)(μ-dppm)$_2$PtCl (M = Fe,[62] Ru[63]). Hence, the difference in the electronic interactions between Ru/Pt and Fe/Pt that results in the potential shift for Pt(II/IV) cannot be detected in the IR data.

Additional studies on CpRu(PPh_3)(μ-I)(μ-dppm)PtI_2 (**14**) show that the more electron-donating ligand triphenylphosphine induces a positive shift of the Ru(II/III) redox couple (about 140 mV) and a negative shift of the Pt(II/IV) redox wave (about 340 mV) for the Ru/Pt complex **14**, in comparison to the carbonyl compound **8**. This behavior suggests that the PPh_3 ligand on Ru leads to stronger electron donation from Ru to the Pt through the I bridge. On the other hand, the iron complex **9** shows very similar behavior compared to the heterobimetallic complex **14**, suggesting that the combination Fe-carbonyl/Pt in complex **9** exhibits equivalent electronic interactions compared to the combination Ru−PPh_3/Pt in complex **14**.

The cyclic voltammograms for the Ru/Pd complex **10** and the Fe/Pd complex **11** exhibit irreversible oxidations at 0.90 and 0.95 V vs NHE, assigned to the Ru(II/III) and Fe(II/III) couples, respectively. The Ru/Pd complex **10** exhibits a quasi-reversible Pd(II/IV) redox wave around 1.79 V vs NHE, which appears as a shoulder on the irreversible Ru(III/IV) wave ($E_{p,a}$ = 1.98 V). As seen for the Fe/Pt complex **9**, significant electron donation through the I bridge is also observed for the Fe/Pd complex **11,** with a quasi-reversible Pd(II/IV) redox wave of **11** that is more easily oxidized by 280 mV ($E_{1/2}$ = 1.51 V) in comparison to the Ru/Pd complex **10**. Comparison of complexes **10** and **11** with the triphenylphosphine Ru/Pd compound **15** shows a trend similar to that for the Pt complexes **8**, **9**, and **14**. The more electron donating triphenylphosphine ligand induces a significant positive shift of the potential of the Ru(II/III) center for **15** in comparison to the shift observed for the Ru/Pt complex **14**. The Ru(II/III) wave of **15** is shifted to higher potential by 390 mV compared to the value for **14**, probably as a consequence of greater electronic donation through the iodide bridge to the Pd center. This observation is consistent with the shift of the Pd(II/IV) wave of **15** to lower potential with respect to the value for the Ru−CO compound **10**. As observed for the analogous Pt complexes **9** and **14**, similar behavior is observed between the Ru−PPh_3/Pd **15** and the Fe−carbonyl/Pd compound **11**.

The Ru/Au complex **12** exhibits irreversible waves at 0.99 and 2.02 V vs NHE for the Ru(II/III) and Ru(III/IV) couples, respectively, and a quasi-reversible wave at 1.72 V for the Au(I/III) couple. This compound was found to be the least stable heterobimetallic complex under the conditions of cyclic voltammetry, with degradation evident after several successive cycles. The cyclic voltammogram of the Fe/Au analogue **13** (Figure 5) also displays three redox waves: two quasi-reversible at 0.92 and 1.49 V vs NHE assigned to the Fe(II/III) and Au(I/III) redox couples, respectively, and an irreversible wave at 1.99 V for the Fe(III/IV) couple. The small wave at 1.13 V corresponds to the redox potential of CpFe(κ^1-dppm)(CO)I (**7**), a degradation product of **13**. As previously observed for CpRu(PPh_3)I(μ-dppm)AuI (**16**),[53] the waves for the non-iodide-bridged Ru/Au and Fe/Au complexes **12** and **13** are very similar to those of the mononuclear compounds CpRu(CO)(PPh_3)I (**4**), CpFe(CO)(PPh_3)I (**5**), and PPh_3AuI (**18**). This is consistent with the IR data, which suggest limited interactions between the two metals of **12** and **13** through the dppm bridge.

UV−Vis Spectroscopy. In order to gain further insight into the electronic structures of these bimetallic complexes, the UV−vis spectra of the heterobimetallic complexes **8**−**13** were recorded in acetonitrile, THF, dichloromethane, and benzene solutions (Table 6) and compared with those of the corresponding monometallic derivatives **6** and **7**. All of the compounds exhibit intense absorptions in the UV range below 270 nm. Similar high-energy bands in half-sandwich complexes bearing phosphine ligands have been assigned to ligand-centered $\pi \rightarrow \pi^*$ electronic transitions.[64]

The spectrum for the mononuclear Ru complex **6** possesses two major features: a low-energy band in the visible region at 436 nm (band I, ϵ = 428 M^{-1} cm^{-1}) and a higher energy band at 324 nm (band II, ϵ = 3140 M^{-1} cm^{-1}). A third band (band III) is also observed around 275 nm, appearing as a shoulder on the higher energy feature. The iron complex **7** shows features similar to those of Ru complex **6**. Complex **7** exhibits a low-energy absorption (band I, 612 nm, ϵ = 191 M^{-1} cm^{-1}) and two absorptions at higher energy (band II, 438 nm, ϵ = 802 M^{-1} cm^{-1}; band III, 385 nm, ϵ = 800 M^{-1} cm^{-1}). These transitions are red-shifted by approximately 176, 114, and 110 nm, respectively, from those of Ru complex **6**, and their extinction coefficients are 2−5 times lower. An analogous effect has been reported for Cp*M(PMe_3)$_2$X (M = Fe, Ru).[65] An additional absorption (band IV, $\epsilon \approx$ 2700 M^{-1} cm^{-1}) is also observed for **7**, on the high-energy side, appearing as a shoulder around 334 nm. The relatively weak intensities of these bands, low solvent dependence, and band shifts to higher energy in the series Fe < Ru[65,66] allows assignment of bands I−IV as d−d transitions.

As expected, the absorption spectra of the bimetallic Ru/Au complex **12** are very similar to those of Ru complex **6** and a similar relationship is observed for the Fe complex **7** and the Fe/Au complex **13**. These results are consistent with those obtained in IR and cyclic voltammetry, once again confirming that the electronic interactions between the two metals through the dppm bridge are negligible.

Previous studies with the PPh_3-substituted compounds Cp(PPh_3)Ru(μ-X)(μ-dppm)MX_2 (M = Pt, Pd) have shown that the heterobimetallic complexes tend to exhibit band structures comparable to those of the corresponding monometallic Ru complexes.[53] These results suggest that the low-energy transitions are localized at the Ru center, with the differences in absorption attributed to the electronic interactions between the two metals. Spectra of the Ru/Pt and Fe/Pt heterobimetallic complexes **8** and **9** are similar to those of **6** and **7**, respectively. Three transitions are observed for the Ru/Pt complex **8**. The first band (band I, 432 nm, ϵ = 3010 M^{-1} cm^{-1}) appears as a shoulder and has an extinction coefficient 7 times that of the monometallic Ru complex **6**. Transitions II and III are similar in intensity to those from the Ru monometallic **6** but are slightly red-shifted. As for the monometallic Fe complex **7**, the Fe/Pt complex **9** exhibits four transitions which are not well resolved. Band I appears as a tail around 571 nm with a relatively low extinction coefficient ($\epsilon \approx$ 270 M^{-1} cm^{-1}), while band II (417 nm, ϵ = 4690 M^{-1} cm^{-1}), band III (350 nm, ϵ = 6450 M^{-1}

(62) Braunstein, P.; Rose, J. In *Metal Clusters in Chemistry*; Braunstein, P., Oro, L. A., Raithby, P. R., Eds.; Wiley-VCH: Weinheim, Germany, 1999; Vol. 2, pp 616−677.

(63) Sterenberg, B. T.; Jennings, M. C.; Puddephatt, R. J. *Organometallics* **1999**, *18*, 3737−3743.

(64) Cordiner, R. L.; Albesa-Jové, D.; Roberts, R. L.; Farmer, J. D.; Puschmann, H.; Corcoran, D.; Goeta, A. E.; Howard, J. A. K.; Low, P. J. *J. Organomet. Chem.* **2005**, *690*, 4908−4919.

(65) Bray, R. G.; Bercaw, J. E.; Gray, H. B.; Hopkins, M. D.; Paciello, R. A. *Organometallics* **1987**, *6*, 922−925.

(66) Gerloch, M.; Constable, E. C. *Transition Metal Chemistry*: *The Valence Shell in d-Block Chemistry*; VCH: Weinheim, Germany, 1994.

Table 6. UV−Vis Spectral Data of Complexes 6−13

		abs, λ_{max}/nm (ϵ/M^{-1} cm^{-1})			
complex	medium	IV	III	II	I
6	benzene		279 (7830) sh	324 (3480)	436 (472)
	THF		276 (8490) sh	325 (3110)	438 (432)
	CH_2Cl_2		275 (9780) sh	324 (3140)	436 (428)
	acetonitrile		276 (9720) sh	324 (3250)	439 (438)
7	benzene	328 (2850) sh	388 (920) sh	439 (860)	612 (193)
	THF	332 (2940)	396 (1130) sh	442 (950)	620 (206)
	CH_2Cl_2	324 (2700) sh	385 (800) sh	438 (802)	612 (191)
	acetonitrile	323 (2430) sh	381 (720) sh	438 (770)	612 (161)
8	benzene		334 (3860) sh	388 (3140) sh	431 (2720)
	THF		328 (8620) sh	387 (4350)	428 (3620) sh
	CH_2Cl_2		335 (7510) sh	388 (4300)	432 (3010) sh
	acetonitrile		331 (5580) sh	384 (3170)	423 (2300) sh
9	benzene	288 (12 120) sh	354 (6190)	438 (3611) sh	tail
	THF	324 sh	391 (5970)	423 (5670) sh	tail
	CH_2Cl_2	321 (9025) sh	350 (6450) sh	417 (4690)	tail
	acetonitrile		326 (7430) sh	404 (3911)	571 (270)
10	benzene	324 (8830)		524 (2050)	624 (660) sh
	THF	327 (14 100)	397 sh	520 (3480)	641 (885) sh
	CH_2Cl_2	330 (18 330)	396 sh	495 (4720)	622 (985) sh
	acetonitrile	329 (17 380)	389 (6320) sh	482 (4300)	618 (816) sh
11	benzene	329 (14 250)	430 (3950) sh	520 (3220)	647 (946) sh
	THF	337 (14 570) sh	424 (4780) sh	513 (4370)	643 (1280) sh
	CH_2Cl_2	351 (11 790) sh	424 (4700) sh	499 (4540)	618 sh
	acetonitrile	352 (12 570) sh	421 (4930) sh	495 (5160)	613 (1840) sh
12	benzene		280 (6600)	308 (3820) sh	414 (215)
	THF		274 (7680) sh	304 (3650) sh	418 (248)
	CH_2Cl_2		274 (8950) sh	304 (3760) sh	418 (245)
	acetonitrile		274 (7920) sh	306 (3350) sh	420 (197) sh
13	benzene	326 (2950) sh	386 (996) sh	442 (741)	607 (182)
	THF	325 (2950)	375 (1660) sh	437 (724)	610 (149)
	CH_2Cl_2	325 (3340) sh	375 (1160) sh	441(814)	611 (199)
	acetonitrile	327 (1430) sh	377 (869) sh	440 (697)	612 (158)

cm^{-1}), and band IV (310 nm, ϵ = 9025 M^{-1} cm^{-1}) are similar to those from complex **7** but exhibit higher intensities. A blue shift of the d−d transitions is generally expected for isostructural compounds when the metal is changed from Fe to Ru, due to increased electronic density at Ru.[65] Comparison of the transitions between the two platinum complexes **8** and **9** reveals the expected blue shift of all the bands. However (except for band I), the intensities are comparable between the Ru/Pt complex **8** and the Fe/Pt complex **9**, which suggests some charge-transfer character associated with the d−d transitions.

The spectrum for the Fe/Pd complex **11** shows features similar to those of the Fe complex **7**, but the transitions are slightly red-shifted and are 5−11 times more intense. Three transitions are observed in the visible region of the spectrum for complex **11**. Band I appears as a shoulder around 613 nm, with an extinction coefficient that is difficult to resolve ($\epsilon \approx$ 946−1840 M^{-1} cm^{-1}), followed by two bands with higher intensities (band II, 499 nm, ϵ = 4540 M^{-1} cm^{-1}; band III, 424 nm, ϵ = 4700 M^{-1} cm^{-1}), while a more intense absorption is also observed in the near-UV region at 351 nm (band IV, ϵ = 11 790 M^{-1} cm^{-1}). A significant difference is observed for Ru/Pd complex **10** as compared to the monometallic Ru complex **6** and the heterobimetallic complexes **8** and **12.** The spectrum of **10** is dominated by two transitions: band II in the visible region (495 nm, ϵ = 4720 M^{-1} cm^{-1}) and band IV, appearing at higher energy (330 nm, ϵ = 18 330 M^{-1} cm^{-1}). Shoulders are also observed on the lower energy sides of band II (band I, 622 nm, ϵ = 985 M^{-1} cm^{-1}) and band IV (band III, 396 nm, $\epsilon \approx$ 6000 M^{-1} cm^{-1}). First of all, the expected blue shift observed for the heterobimetallic Ru/Pt and Fe/Pt pair **8** and **9** as well as that for the heterobimetallic Ru/Au and Fe/Au pair **12** and **13** is not observed for complexes **10** and **11**. In fact, the transitions for the Ru/Pd complex **10** are red-shifted with respect to those of the model compound **6** and the Ru/Pt complex **8**, which makes them similar to those from the Fe/Pd complex **11**. These spectral characteristics for complex **10** are consistent with charge-transfer transitions. Also consistent with MLCT is the presence of a solvatochromic effect[67,68] for band II of complexes **10** and **11**, in which a blue shift of the maximum absorption is observed when the polarity of the solvent increases. These results are consistent with a major role for the iodide bridge in the electronic structure of the compounds, since the non-iodide-bridged complexes **12** and **13** exhibit spectra very similar to those of the monometallic complexes **6** and **7**.

Conclusion

In summary, this work describes the synthesis and characterization of a new series of heterobimetallic Ru/Pt, Ru/Pd, and Ru/Au complexes as well as their isoelectronic Fe/Pt, Fe/Pd, and Fe/Au analogues. The structures of compounds **8**−**11** were determined by X-ray crystallography and were found to be similar to those of previously reported halide-bridged complexes.

The heterobimetallic complexes **8**−**11** also illustrate the effect of an I-bridged ligand in mediating the electronic interactions between the two metals, as can be seen by comparison of the

(67) Szklarzewicz, J.; Makula, A.; Matoga, D.; Fawcett, J. *Inorg. Chem. Acta* **2005**, *358*, 1749−1761.
(68) Fischer, H.; Szesni, N. *Coord. Chem. Rev.* **2004**, *248*, 1659−1677.

redox potentials, carbonyl stretching frequencies, and UV−vis transitions of heterobimetallic complexes **8**−**11** with those of the monometallic compounds **4**−**7** and also with those of the dppm-bridged complexes **12** and **13**. Investigations on methanol oxidation studies using these complexes will be reported in due course.

Acknowledgment. This work was supported by NASA Glenn Research Center under Grant No. NAG 3-2930. K.A.A. wishes to acknowledge the National Science Foundation and the University of Florida for funding of the purchase of the X-ray equipment. C.R.H. thanks the Arnold and Mabel Beckman Foundation for support. We thank Christophe R. G. Grenier for helpful discussions.

Supporting Information Available: Text, tables, figures, and CIF files giving experimental procedures for X-ray crystallography, crystallographic data for **6**−**9** (including atomic coordinates, bond lengths and angles, and anisotropic displacement parameters), and ^{1}H and $^{31}P\{^{1}H\}$ NMR spectra for **13**. This material is available free of charge via the Internet at http://pubs.acs.org.

OM0610750